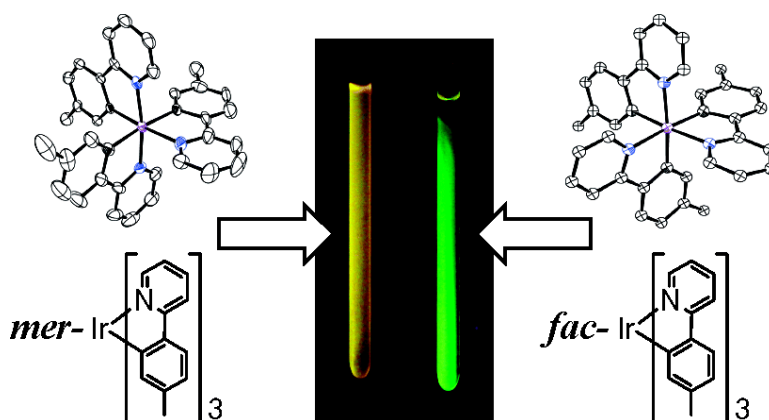


## Synthesis and Characterization of Facial and Meridional Tris-cyclometalated Iridium(III) Complexes

Arnold B. Tamayo, Bert D. Alleyne, Peter I. Djurovich, Sergey Lamansky, Irina Tsyba, Nam N. Ho, Robert Bau, and Mark E. Thompson

*J. Am. Chem. Soc.*, **2003**, 125 (24), 7377-7387 • DOI: 10.1021/ja034537z • Publication Date (Web): 22 May 2003

Downloaded from <http://pubs.acs.org> on March 29, 2009



### More About This Article

Additional resources and features associated with this article are available within the HTML version:

- Supporting Information
- Links to the 70 articles that cite this article, as of the time of this article download
- Access to high resolution figures
- Links to articles and content related to this article
- Copyright permission to reproduce figures and/or text from this article

[View the Full Text HTML](#)

## Synthesis and Characterization of Facial and Meridional Tris-cyclometalated Iridium(III) Complexes

Arnold B. Tamayo, Bert D. Alleyne, Peter I. Djurovich, Sergey Lamansky, Irina Tsyba, Nam N. Ho, Robert Bau, and Mark E. Thompson\*

Contribution from the Department of Chemistry, University of Southern California, Los Angeles, California 90089-0744

Received February 6, 2003; E-mail: met@usc.edu

**Abstract:** The synthesis, structures, electrochemistry, and photophysics of a series of facial (*fac*) and meridional (*mer*) tris-cyclometalated Ir(III) complexes are reported. The complexes have the general formula  $\text{Ir}(\text{C}^{\wedge}\text{N})_3$  [where  $\text{C}^{\wedge}\text{N}$  is a monoanionic cyclometalating ligand; 2-phenylpyridyl (*ppy*), 2-(*p*-tolyl)pyridyl (*tpy*), 2-(4,6-difluorophenyl)pyridyl (*46dfppy*), 1-phenylpyrazolyl (*ppz*), 1-(4,6-difluorophenyl)pyrazolyl (*46dfppz*), or 1-(4-trifluoromethylphenyl)pyrazolyl (*tfmppz*)]. Reaction of the dichloro-bridged dimers  $[(\text{C}^{\wedge}\text{N})_2\text{Ir}(\mu\text{-Cl})_2\text{Ir}(\text{C}^{\wedge}\text{N})_2]$  with 2 equiv of  $\text{HC}^{\wedge}\text{N}$  at 140–150 °C forms the corresponding meridional isomer, while higher reaction temperatures give predominantly the facial isomer. Both facial and meridional isomers can be obtained in good yield (>70%). The meridional isomer of  $\text{Ir}(\text{tpy})_3$  and facial and meridional isomers of  $\text{Ir}(\text{ppz})_3$  and  $\text{Ir}(\text{tfmppz})_3$  have been structurally characterized using X-ray crystallography. The facial isomers have near identical bond lengths (av Ir–C = 2.018 Å, av Ir–N = 2.123 Å) and angles. The three meridional isomers have the expected bond length alternations for the differing trans influences of phenyl and pyridyl/pyrazolyl ligands. Bonds that are trans to phenyl groups are longer (Ir–C av = 2.071 Å, Ir–N av = 2.031 Å) than when they are trans to heterocyclic groups. The Ir–C and Ir–N bonds with trans N and C, respectively, have bond lengths very similar to those observed for the corresponding facial isomers. DFT calculations of both the singlet (ground) and the triplet states of the compounds suggest that the HOMO levels are a mixture of Ir and ligand orbitals, while the LUMO is predominantly ligand-based. All of the complexes show reversible oxidation between 0.3 and 0.8 V, versus  $\text{Fc}/\text{Fc}^+$ . The meridional isomers are easier to oxidize by ca. 50–100 mV. The phenylpyridyl-based complexes have reduction potentials between –2.5 and –2.8 V, whereas the phenylpyrazolyl-based complexes exhibit no reduction up to the solvent limit of –3.0 V. All of the compounds have intense absorption bands in the UV region assigned into  $^1(\pi \rightarrow \pi^*)$  transitions and weaker MLCT (metal-to-ligand charge transfer) transitions that extend to the visible region. The MLCT transitions of the pyrazolyl-based complexes are hypsochromically shifted relative to those of the pyridyl-based compounds. The phenylpyridyl-based Ir(III) tris-cyclometalates exhibit intense emission both at room temperature and at 77 K, whereas the phenylpyrazolyl-based derivatives emit strongly only at 77 K. The emission energies and lifetimes of the phenylpyridyl-based complexes (450–550 nm, 2–6  $\mu\text{s}$ ) and phenylpyrazolyl-based compounds (390–440 nm, 14–33  $\mu\text{s}$ ) are characteristic for a mixed ligand-centered/MLCT excited state. The meridional isomers for both pyridyl and pyrazolyl-based cyclometalates show markedly different spectroscopic properties than do the facial forms. Isolated samples of *mer*- $\text{Ir}(\text{C}^{\wedge}\text{N})_3$  complexes can be thermally and photochemically converted to facial forms, indicating that the meridional isomers are kinetically favored products. The lower thermodynamic stabilities of the meridional isomers are likely related to structural features of these complexes; that is, the meridional configuration places strongly trans influencing phenyl groups opposite each other, whereas all three phenyl groups are opposite pyridyl or pyrazolyl groups in the facial complexes. The strong trans influence of the phenyl groups in the meridional isomers leads to the observation that they are easier to oxidize, exhibit broad, red-shifted emission, and have lower quantum efficiencies than their facial counterparts.

### Introduction

A significant research effort has focused on the synthesis and photophysical characterization of octahedral  $4d^6$  and  $5d^6$  metal complexes.<sup>1</sup> These  $d^6$  complexes, particularly the diimine (i.e., bipyridine, phenanthroline) chelates of Ru(II) and Os(II), have been widely used in a variety of photonic applications, including photocatalysis and photoelectrochemistry.<sup>2,3</sup> The attraction of these  $d^6$  complexes for such applications comes from their long

excited-state lifetimes and high luminescent efficiencies. These properties increase the likelihood of either an energy or an electron-transfer process occurring prior to a radiative or

- (1) (a) Balzani, V.; Scandola, F. *Supramolecular Photochemistry*; Ellis Horwood: Chichester, U.K., 1991. (b) Balzani, V.; Credi, A.; Scandola, F. In *Transition Metals in Supramolecular Chemistry*; Fabrizzi, L., Poggi, A., Eds.; Kluwer: Dordrecht, The Netherlands, 1994; p 1. (c) Lehn, J.-M. *Supramolecular Chemistry-Concepts and Properties*; VCH: Weinheim, Germany, 1995. (d) Bignozzi, C. A.; Schoonover, J. R.; Scandola, F. *Prog. Inorg. Chem.* **1997**, *44*, 11.

nonradiative relaxation. The photophysics of related tris-chelate Ir(III) complexes have also been investigated.<sup>4–6</sup> These Ir(III) complexes have been prepared with either diimine ligands or cyclometalated ligands, such as 2-phenylpyridinato-C<sup>2</sup>,N (*ppy*)<sup>5,6</sup> and 2,2-thienylpyridinato-C<sup>2</sup>,N (*thpy*).<sup>6</sup> Complexes with the formally monoanionic cyclometalating ligands are isoelectronic with the cationic tris-diimine complexes of Ru(II) and Os(II). As compared to Ru(II) and Os(II) complexes, however, the d<sup>6</sup> Ir(III) complexes exhibit longer excited-state lifetimes, typically in the order of microseconds, and higher luminescence efficiencies [e.g.,  $\phi_{\text{phos}}$  (*fac*-Ir(*ppy*)<sub>3</sub>) = 0.4]<sup>7</sup> in fluid solutions. These properties are due to efficient intersystem crossing between the singlet and triplet excited states brought about by the strong spin-orbit coupling of the Ir(III) metal ion.

The photophysical properties of bis- and tris-cyclometalated complexes of Ir(III) make them very useful for several photonic applications.<sup>4,5a,8–10</sup> These compounds can be employed as sensitizers for outer-sphere electron-transfer reactions,<sup>11,12</sup> photocatalysts for CO<sub>2</sub> reduction,<sup>13</sup> photooxidants, and singlet oxygen sensitizers.<sup>14</sup> A recent application for these compounds is in the field of organic light-emitting devices (OLEDs), where they have been used as phosphorescent dopants in the emitting layer.<sup>8b</sup> The singlet and triplet excited states that are created during charge recombination are trapped at the phosphor, where the effective intersystem crossing leads to efficient electrophosphorescence at room temperature.<sup>15</sup> Recently, it has also been

shown that a phenylpyrazolyl-based Ir(III) tris-cyclometalate can be used as an electron blocking material (preventing electron leakage to the hole-transporting layer) to make highly efficient single-dopant white OLEDs.<sup>16</sup>

Metal d<sup>6</sup> tris-complexes with asymmetric chelate ligands can have either a facial (*fac*) or a meridional (*mer*) configuration. The photophysical and electrochemical properties of facial and meridional isomers have been investigated for a number of Ru(II) complexes having asymmetric diimine ligands.<sup>17–21</sup> However, for these cationic Ru(II) diimine complexes, it has been difficult to achieve control over which isomer is obtained from the synthesis, as well as to isolate and purify a specific isomer.<sup>17–20</sup> Moreover, the class of ligands that have been used (e.g., pyridyl-pyrazoles) gave only minor differences in the photophysical properties between the facial and meridional isomers because the two types of coordinating ligand, that is, pyridyl and pyrazolyl, have very similar electronic and coordinating characteristics.<sup>17,18</sup> On the other hand, tris-chelates with cyclometalating ligands such as 2-phenylpyridyl should have pronounced differences between the facial and meridional isomers due to the marked disparity between the formally anionic phenyl ligand and neutral pyridyl ligand. To date, all investigations into the synthesis and photophysics of tris-cyclometalated metal d<sup>6</sup> complexes have been reported on the facial isomers,<sup>5b,h,6,9a,10</sup> whereas the chemistry of the meridional analogues has remained unexplored. Herein, we describe new synthetic routes which allow for isolation of either facial or meridional isomers of tris-cyclometalates of Ir(III). The meridional isomers have been prepared in good yield (ca. >70%) as kinetically favored products. The structures of these complexes have been determined by X-ray diffraction and NMR methods. The photophysical properties of both facial and meridional complexes have also been examined and show distinct differences between the two forms. The meridional isomers display red-shifted emission and decreased quantum efficiencies relative to their facial analogues. We also report on the conversion of the meridional isomers to facial forms by both thermal and photochemical routes.

## Experimental Section

**Equipment.** UV–visible spectra were measured on an AVIV model 14DS UV–vis–IR (a reengineered Cary 14) or a Hewlett-Packard 4853 diode array spectrophotometer. Steady-state emission spectra were measured with a Photon Technology International QuantaMaster model C-60 spectrofluorimeter. Phosphorescence lifetime measurements (>2  $\mu$ s) were performed on the same fluorimeter equipped with a microsecond xenon flash lamp or using an IBH Fluorocube fluorimeter equipped with a blue LED ( $\lambda_{\text{max}}$  = 373 nm). The quantum efficiency (QE) measurements were carried out at room temperature in degassed 2-methyltetrahydrofuran solutions using the optically dilute method.<sup>22</sup>

- (2) (a) Kalyanasundaram, K. *Coord. Chem. Rev.* **1982**, *46*, 159. (b) Chin, K.-F.; Cheung, K.-K.; Yip, H.-K.; Mak, T. C. W.; Che, C. M. *J. Chem. Soc., Dalton Trans.* **1995**, *4*, 657. (c) Sonoyama, N.; Karasawa, O.; Kaizu, Y. *J. Chem. Soc., Faraday Trans.* **1995**, *91*, 437. (d) Tan-Sien-Hee, L.; Mesmaeker, A. K.-D. *J. Chem. Soc., Dalton Trans.* **1994**, *24*, 3651. (e) Kalyanasundaram, K.; Gratzel, M. *Coord. Chem. Rev.* **1998**, *177*, 347.
- (3) (a) Anderson, P. A.; Anderson, R. F.; Furue, M.; Junk, P. C.; Keene, F. R.; Patterson, B. T.; Yeomans, B. D. *Inorg. Chem.* **2000**, *39*, 2721. (b) Li, C.; Hoffman, M. Z. *Inorg. Chem.* **1998**, *37*, 830. (c) Berg-Brennan, C.; Subramanian, P.; Absi, M.; Stern, C.; Hupp, J. T. *Inorg. Chem.* **1996**, *35*, 3719. (d) Kawanishi, Y.; Kitamura, N.; Tazuke, S. *Inorg. Chem.* **1989**, *28*, 2968.
- (4) (a) Balzani, V.; Juris, A.; Venturi, M.; Campagna, S.; Serroni, S. *Chem. Rev.* **1996**, *96*, 759. (b) Shaw, J. R.; Sadler, G. S.; Wacholtz, W. F.; Ryu, C. K.; Schmehl, R. H. *New J. Chem.* **1996**, *20*, 749.
- (5) (a) Sprouse, S.; King, K. A.; Spellane, P. J.; Watts, R. J. *J. Am. Chem. Soc.* **1984**, *106*, 6647. (b) King, K. A.; Spellane, P. J.; Watts, R. J. *J. Am. Chem. Soc.* **1985**, *107*, 1432. (c) Ohsawa, Y.; Sprouse, S.; King, K. A.; DeArmond, M. K.; Hanck, K. W.; Watts, R. J. *J. Phys. Chem.* **1987**, *91*, 1047. (d) Ichimura, K.; Kobayashi, T.; King, K. A.; Watts, R. J. *J. Phys. Chem.* **1987**, *91*, 6104. (e) Garces, F. O.; King, K. A.; Watts, R. J. *Inorg. Chem.* **1988**, *27*, 3464. (f) Garces, F. O.; Watts, R. J. *Inorg. Chem.* **1990**, *29*, 582. (g) Wilde, A. P.; King, K. A.; Watts, R. J. *J. Phys. Chem.* **1991**, *95*, 629. (h) Dedeian, K.; Djurovich, P. I.; Garces, F. O.; Carlson, G.; Watts, R. J. *Inorg. Chem.* **1991**, *30*, 1685.
- (6) (a) Colombo, M. G.; Hauser, A.; Gudel, H. U. *Inorg. Chem.* **1993**, *32*, 3088. (b) Colombo, M. G.; Brunold, T. C.; Riedener, T.; Gudel, H. U. *Inorg. Chem.* **1994**, *33*, 545.
- (7) (a) Sprouse, S.; King, K. A.; Spellane, P. J.; Watts, R. J. *J. Am. Chem. Soc.* **1984**, *106*, 6647. (b) Crosby, G. A. *J. Chim. Phys.* **1967**, *64*, 160.
- (8) (a) Lamansky, S.; Djurovich, P.; Murphy, D.; Abdel-Razzaq, F.; Kwong, R.; Tsyba, I.; Bortz, M.; Mui, B.; Bau, R.; Thompson, M. E. *Inorg. Chem.* **2001**, *40*, 1704. (b) Lamansky, S.; Djurovich, P.; Murphy, D.; Abdel-Razzaq, F.; Lee, H.; Adachi, C.; Burrows, P. E.; Forrest, S. R.; Thompson, M. E. *Inorg. J. Am. Chem. Soc.* **2001**, *40*, 1704.
- (9) (a) Grushin, V. V.; Herron, N.; LeCloux, D. D.; Marshall, W. J.; Petrov, V. A.; Wang, Y. *Chem. Commun.* **2001**, 1494. (b) Wang Y.; Herron, N.; Grushin, V. V.; LeCloux, D.; Petrov, V. *Appl. Phys. Lett.* **2001**, *79*, 479.
- (10) Ostrowski, J. C.; Robinson, M. R.; Heeger, A. J.; Bazan, G. C. *Chem. Commun.* **2002**, 784.
- (11) (a) Sutin, N. *Acc. Chem. Res.* **1968**, *1*, 225. (b) Meyer, T. J. *Acc. Chem. Res.* **1978**, *11*, 94.
- (12) Schmid, B.; Garces, F. O.; Watts, R. J. *Inorg. Chem.* **1994**, *32*, 9.
- (13) (a) Belmore, K. A.; Vanderpool, R. A.; Tsai, J.-C.; Khan, M. A.; Nicholas, K. M. *J. Am. Chem. Soc.* **1988**, *110*, 2004. (b) Silaware, N. D.; Goldman, A. S.; Ritter, R.; Tyler, D. R. *Inorg. Chem.* **1989**, *28*, 1231.
- (14) (a) Demas, J. N.; Harris, E. W.; McBride, R. P. *J. Am. Chem. Soc.* **1977**, *99*, 3547. (b) Demas, J. N.; Harris, E. W.; Flynn, C. M.; Diemente, D. J. *Am. Chem. Soc.* **1975**, *97*, 3838. (c) Gao, R.; Ho, D. G.; Hernandez, B.; Selke, M.; Murphy, D.; Djurovich, P. I.; Thompson, M. E. *J. Am. Chem. Soc.* **2002**, *124*, 14828.
- (15) (a) Baldo, M. A.; O'Brien, D. F.; You, Y.; Shoustikov, A.; Sibley, S.; Thompson, M. E.; Forrest, S. R. *Nature* **1998**, *395*, 151. (b) Baldo, M. A.; Lamansky, S.; Burrows, P. E.; Thompson, M. E.; Forrest, S. R. *Appl. Phys. Lett.* **1999**, *75*, 4. (c) Thompson, M. E.; Burrows, P. E.; Forrest, S. R. *Curr. Opin. Solid State Mater. Sci.* **1999**, *4*, 369.
- (16) Adamovich, V.; Brooks, J.; Tamayo, A.; Djurovich, P.; Alexander, A.; Thompson, M. E. *New J. Chem.* **2002**, 1171.
- (17) Steel, P. J.; Lahousse, F.; Lerner, D.; Marzin, C. *Inorg. Chem.* **1983**, *22*, 1488.
- (18) Steel, P. J.; Constable, E. C. *J. Chem. Soc., Dalton Trans.* **1990**, 1389.
- (19) Luo, Y.; Potvin, P. G.; Tse, Y.; Lever, A. B. P. *Inorg. Chem.* **1996**, *35*, 5445.
- (20) Fletcher, N. C.; Nieuwenhuysen, M.; Rainey, S. *J. Chem. Soc., Dalton Trans.* **2001**, 2641.
- (21) Fletcher, N. C.; Nieuwenhuysen, M.; Prabakaran, R.; Wilson, A. *Chem. Commun.* **2002**, 1188.

**Table 1.** Crystallographic Data for *mer*-Ir(*tpy*)<sub>3</sub>, *fac*-Ir(*ppz*)<sub>3</sub>, *mer*-Ir(*ppz*)<sub>3</sub>, *fac*-Ir(*tfmppz*)<sub>3</sub>, and *mer*-Ir(*tfmppz*)<sub>3</sub>

|   | <i>mer</i> -Ir( <i>tpy</i> ) <sub>3</sub> ·CH <sub>2</sub> Cl <sub>2</sub>        | <i>fac</i> -Ir( <i>ppz</i> ) <sub>3</sub>          | <i>mer</i> -Ir( <i>ppz</i> ) <sub>3</sub>          | <i>fac</i> -Ir( <i>tfmppz</i> ) <sub>3</sub>                    | <i>mer</i> -Ir( <i>tfmppz</i> ) <sub>3</sub>                    |
|---|---|--|--|---|---|
| empirical formula                                   | C <sub>36</sub> H <sub>30</sub> IrN <sub>3</sub> ·CH <sub>2</sub> Cl <sub>2</sub> | C <sub>27</sub> H <sub>21</sub> IrN <sub>6</sub>   | C <sub>27</sub> H <sub>21</sub> IrN <sub>6</sub>   | C <sub>30</sub> H <sub>18</sub> F <sub>9</sub> IrN <sub>6</sub> | C <sub>30</sub> H <sub>18</sub> F <sub>9</sub> IrN <sub>6</sub> |
| formula weight                                      | 781.76  | 621.70   | 621.70   | 825.70  | 825.70  |
| temperature, K                                      | 223(2)  | 273(2)   | 296(2)   | 296(2)  | 296(2)  |
| wavelength (Å)                                      | 0.71073   | 0.71073  | 0.71073  | 0.71073   | 0.71073   |
| crystal system                                      | monoclinic  | tetragonal   | monoclinic   | orthorhombic  | monoclinic  |
| space group   | <i>P</i> 2(1)/ <i>n</i>   | <i>P</i> -42(1) <i>c</i>                           | <i>P</i> 2(1)/ <i>c</i>                            | <i>Pbca</i>   | <i>P</i> 2(1)/ <i>n</i>   |
| unit cell dimensions                                |   |  |  |   |   |
| <i>a</i> (Å)  | 15.113(2)   | 23.125(11)   | 15.2907(13)  | 17.5088(13)   | 11.5923(10)   |
| <i>b</i> (Å)  | 9.9696(15)  | 23.125(11)   | 14.8863(11)  | 17.0833(12)   | 33.878(3)   |
| <i>c</i> (Å)  | 21.093(3)   | 8.854(8)   | 10.1503(9)   | 40.472(3)   | 15.5667(14)   |
| α (deg)   | 90  | 90   | 90   | 90  | 90  |
| β (deg)   | 91.383(3)   | 90   | 97.607(5)  | 90  | 103.030(2)  |
| γ (deg)   | 90  | 90   | 90   | 90  | 90  |
| volume (Å <sup>3</sup> )                            | 3177.2(8)   | 4735(5)  | 2290.1(3)  | 12 105.4(15)  | 5956.0(9)   |
| <i>Z</i>  | 4   | 8  | 4  | 16  | 8   |
| density, calcd (g/cm <sup>3</sup> )                 | 1.634   | 1.744  | 1.803  | 1.812   | 1.842   |
| absorption coefficient (mm <sup>-1</sup> )          | 4.401   | 5.667  | 5.858  | 4.499   | 4.572   |
| <i>F</i> (000)                                      | 1544  | 2416   | 1208   | 6368  | 3184  |
| θ range for data collection (deg)                   | 1.64–24.71  | 1.25–27.56   | 1.34–28.42   | 1.01–24.71  | 1.47–24.71  |
| reflections collected                               | 24 547  | 27 943   | 13 642   | 59 022  | 30 328  |
| independent reflections                             | 5422  | 5315   | 5263   | 10 321  | 10 165  |
|   | [ <i>R</i> (int) = 0.0489]  | [ <i>R</i> (int) = 0.0484]                         | [ <i>R</i> (int) = 0.0262]                         | [ <i>R</i> (int) = 0.0459]                                      | [ <i>R</i> (int) = 0.0313]                                      |
| refinement method                                   | full-matrix least-squares on <i>F</i> <sup>2</sup>                                | full-matrix least-squares on <i>F</i> <sup>2</sup> | full-matrix least-squares on <i>F</i> <sup>2</sup> | full-matrix least-squares on <i>F</i> <sup>2</sup>              | full-matrix least-squares on <i>F</i> <sup>2</sup>              |
| data/restraints/parameters                          | 5219/0/353  | 5315/0/308   | 5263/0/143   | 10 321/108/786  | 10 165/108/786  |
| goodness-of-fit on <i>F</i> <sup>2</sup>            | 1.066   | 1.054  | 1.004  | 1.037   | 1.023   |
| final <i>R</i> indices [ <i>I</i> > 2σ( <i>I</i> )] | 0.0521  | 0.0366   | 0.0480   | 0.0495  | 0.0468  |
| <i>R</i> indices (all data)                         | 0.0686  | 0.0477   | 0.0706   | 0.0731  | 0.0595  |

Solutions of coumarin 47 in ethanol ( $\Phi = 0.60$ ) were used as reference. NMR spectra were recorded on Bruker AMX 360 and 500 MHz instruments. Mass spectra were taken with a Hewlett-Packard GC/MS instrument with electron impact ionization and model 5873 mass sensitive detector. Elemental analyses (CHN) were performed at the Microanalysis Laboratory at the University of Illinois, Urbana-Champaign.

**Electrochemistry.** Cyclic voltammetry and differential pulsed voltammetry were performed using an EG&G potentiostat/galvanostat model 283. Anhydrous DMF (Aldrich) was used as the solvent under inert atmosphere, and 0.1 M tetra(*n*-butyl)ammonium hexafluorophosphate was used as the supporting electrolyte. A glassy carbon rod was used as the working electrode, a platinum wire was used as the counter electrode, and a silver wire was used as a pseudoreference electrode. The redox potentials are based on values measured from differential pulsed voltammetry and are reported relative to a ferrocene/ferrocenium (Cp<sub>2</sub>Fe/Cp<sub>2</sub>Fe<sup>+</sup>) redox couple used as an internal reference,<sup>23</sup> while electrochemical reversibility was determined using cyclic voltammetry.

**X-ray Crystallography.** Diffraction data for *mer*-Ir(*ppz*)<sub>3</sub>, *fac*-Ir(*tfmppz*)<sub>3</sub>, and *mer*-Ir(*tfmppz*)<sub>3</sub> were collected at room temperature (*T* = 23 °C), while data for *mer*-Ir(*tpy*)<sub>3</sub> and *fac*-Ir(*ppz*)<sub>3</sub> were taken at –50 and 0 °C, respectively. The data sets were collected on a Bruker SMART APEX CCD diffractometer with graphite monochromated Mo Kα radiation ( $\lambda = 0.71073$  Å). The cell parameters for the Ir complexes were obtained from a least-squares refinement of the spots (from 60 collected frames) using the SMART program. One hemisphere of crystal data for each compound was collected up to a resolution of 0.80 Å, and the intensity data were processed using the Saint Plus program. All of the calculations for the structure determination were carried out using the SHELXTL package (version 5.1).<sup>24</sup> Absorption corrections were applied by using SADABS.<sup>25</sup> In most cases, hydrogen positions

were input and refined in a riding manner along with the attached carbons. All of the structural analyses proceeded smoothly except that of *mer*-Ir(*ppz*)<sub>3</sub>, which was complicated by a slight packing disorder of one of the three *ppz* ligands. This necessitated several data sets to be collected for *mer*-Ir(*ppz*)<sub>3</sub> until a crystal was found that yielded a satisfactory result. Anisotropic refinement of this data set led to unreasonable bond distances so only the isotropically refined data were used in the subsequent analysis. A summary of the refinement details and the resulting factors for *mer*-Ir(*tpy*)<sub>3</sub>, *fac*-Ir(*ppz*)<sub>3</sub>, *mer*-Ir(*ppz*)<sub>3</sub>, Ir-(*tfmppz*)<sub>3</sub>, and *mer*-Ir(*tfmppz*)<sub>3</sub> are given in Table 1.

**Density Functional Calculations.** DFT calculations were performed using the Titan software package (Wavefunction, Inc.) at the B3LYP/LACVP\*\* level. The HOMO and LUMO energies were determined using minimized singlet geometries to approximate the ground state. The minimized singlet geometries were used to calculate the triplet molecular orbitals and approximate the triplet HSOMO (HSOMO = highest singly occupied molecular orbital).

**Synthesis.** The compounds 2-(4,6-difluorophenyl)pyridine,<sup>26</sup> 1-(4,6-difluorophenyl)pyrazole,<sup>27</sup> and 1-(4-trifluoromethylphenyl)pyrazole<sup>27</sup> were prepared following literature procedures. Ir(*acac*)<sub>3</sub> was purchased from Strem Chemical Co., IrCl<sub>3</sub>·*n*H<sub>2</sub>O was from Next Chimica, and all other chemicals were purchased from Aldrich Chemical Co. and used as received.

All experiments involving IrCl<sub>3</sub>·*n*H<sub>2</sub>O or any other Ir(III) species were carried out in inert atmosphere despite the stability of the compounds in air, the main concern being their oxidative and thermal stability of intermediate complexes at the high temperatures used in the reactions. Cyclometalated Ir(III)  $\mu$ -chloro-bridged dimers of general formula (C<sup>*N*</sup>)<sub>2</sub>Ir( $\mu$ -Cl)<sub>2</sub>Ir(C<sup>*N*</sup>)<sub>2</sub> (where C<sup>*N*</sup> represents a cyclometalating ligand) were synthesized by the method reported by Nonoyama,<sup>28</sup> which involves heating IrCl<sub>3</sub>·H<sub>2</sub>O to 110 °C with 2–2.5 equiv of cyclometalating ligand in a 3:1 mixture of 2-ethoxyethanol and deionized water. (C<sup>*N*</sup>)<sub>2</sub>Ir(O<sup>*O*</sup>) (where O<sup>*O*</sup> represents 2,2,6,6-

(22) (a) Demas, J. N.; Crosby, G. A. *J. Phys. Chem.* **1978**, *82*, 991. (b) DePriest, J.; Zheng, G. Y.; Goswami, N.; Eichhorn, D. M.; Woods, C.; Rillema, D. P. *Inorg. Chem.* **2000**, *39*, 1955.

(23) (a) Gagne, R. R.; Koval, C. A.; Lisensky, G. C. *Inorg. Chem.* **1980**, *19*, 2854. (b) Sawyer, D. T.; Sobkowiak, A.; Roberts, J. L., Jr. *Electrochemistry for Chemists*, 2nd ed.; John Wiley and Sons: New York, 1995; p 467.

(24) Sheldrick, G. M. *SHELXTL*, version 5.1; Bruker Analytical X-ray System, Inc.: Madison, WI, 1997.

(25) Blessing, R. H. *Acta Crystallogr.* **1995**, *A51*, 33.

(26) Lohse, O.; Thevenin, P.; Waldvogel, E. *Synlett* **1999**, *1*, 45.

(27) Finar, I. L.; Rackham, D. M. *J. Chem. Soc. B* **1968**, 211.

(28) Nonoyama, M. *Bull. Chem. Soc. Jpn.* **1974**, *47*, 767.



tetramethyl-3,5-heptanedione, dipivaloylmethane — dpm) was prepared by reacting the dimers with 2–2.5 equiv of the chelating diketone and an equivalent amount of  $K_2CO_3$  in 1,2-dichloroethane at 90 °C for 24 h.<sup>8</sup>

**Synthesis of *fac*-Ir(*C^N*)<sub>3</sub> Complexes. General Procedure. *fac*-Ir(*ppy*)<sub>3</sub>, *fac*-Ir(*46dfppz*)<sub>3</sub>, *fac*-Ir(*tfmppz*)<sub>3</sub>, Method A.** This method involves treating Ir(*acac*)<sub>3</sub> (*acac* = acetylacetonate) with 3–3.5 equiv of the appropriate cyclometalating ligand in refluxing glycerol, as previously described (see eq 1).<sup>5h</sup>

***fac*-Ir(*46dfppy*)<sub>3</sub>, *fac*-Ir(*46dfppz*)<sub>3</sub>, *fac*-Ir(*tfmppz*)<sub>3</sub>, Method B.** The (*C^N*)<sub>2</sub>Ir(*O^O*) complex and 1.2–1.5 equiv of the appropriate cyclometalating ligand were refluxed under inert gas atmosphere in 10 mL of glycerol for 20–24 h. After the mixture was cooled to room temperature, 20 mL of 5% HCl solution was added, and the product was thrice extracted with 25 mL of  $CH_2Cl_2$ . The organic extracts were combined and then dried with anhydrous  $MgSO_4$ , after which the solvent was removed in vacuo. The crude material was then flash chromatographed on a silica column using dichloromethane to yield 60–80% product (see eq 2).

***fac*-Ir(*ppy*)<sub>3</sub>, *fac*-Ir(*tpy*)<sub>3</sub>, *fac*-Ir(*ppz*)<sub>3</sub>, Method C.** [(*C^N*)<sub>2</sub>IrCl]<sub>2</sub> complex, 2–2.5 equiv of the appropriate cyclometalating ligand, and 5–10 equiv of  $K_2CO_3$  were heated to ~200 °C under inert atmosphere in 10 mL of glycerol for 20–24 h. After the mixture was cooled to room temperature, 20 mL of deionized  $H_2O$  was added, and the resulting precipitate was filtered off, washed with two portions of methanol, followed by ether and hexanes. The crude product was then flash chromatographed on a silica column using dichloromethane to yield 65–80% pure *fac*-Ir(*C^N*)<sub>3</sub> (see eq 3).

**Synthesis of *mer*-Ir(*C^N*)<sub>3</sub> Complexes. General Procedure. *mer*-Ir(*ppy*)<sub>3</sub>, *mer*-Ir(*tpy*)<sub>3</sub>, *mer*-Ir(*ppz*)<sub>3</sub>, *mer*-Ir(*46dfppz*)<sub>3</sub>, *mer*-Ir(*tfmppz*)<sub>3</sub>.** All of the meridional isomers, except *mer*-Ir(*46dfppy*)<sub>3</sub>, were prepared by using a modified version of Method C. [(*C^N*)<sub>2</sub>IrCl]<sub>2</sub> complex, 2–2.5 equiv of the appropriate cyclometalating ligand, and 5–10 equiv of  $K_2CO_3$  were heated to 140–145 °C under inert atmosphere in 10 mL of glycerol for 20–24 h. After the mixture was cooled to room temperature, distilled water was added, and the resulting precipitate was filtered off, washed with two more portions of distilled water, and air-dried. The crude product was then flash chromatographed on a silica column using dichloromethane to give 68–80% (based on the starting dichloro-bridged dimer) of the pure meridional tris-cyclometalated complex.

***mer*-Ir(*46dfppy*)<sub>3</sub>.** This complex was prepared by dissolving the corresponding dimer, 2 equiv of ligand, and  $K_2CO_3$  in 2-ethoxyethanol and heated to 120 °C for overnight. The reaction mixture was then allowed to cool to room temperature, and the solvent was removed in vacuo. The crude product mixture was then flash chromatographed on a silica column using dichloromethane to give 74% pure *mer*-Ir(*46dfppy*)<sub>3</sub>.

**Characterization.** <sup>1</sup>H and <sup>13</sup>C NMR chemical shifts and coupling constants for all of the complexes listed below are given in the Supporting Information.

***fac*-Ir(*ppy*)<sub>3</sub> (Method C):** *fac*-tris(2-phenylpyridinato,N,C<sup>2'</sup>)iridium(III). Yield: 79%. <sup>1</sup>H and <sup>13</sup>C NMR spectroscopy and C, H, N analysis match that reported for *fac*-Ir(*ppy*)<sub>3</sub>.<sup>5h</sup>

***fac*-Ir(*tpy*)<sub>3</sub> (Method C):** *fac*-tris(2-(*p*-tolyl)pyridinato,N,C<sup>2'</sup>)iridium(III). Yield: 81%. MS: *m/z* calcd 696.9; found 697. Anal. Calcd for  $C_{36}H_{30}N_3Ir$ : C, 62.05; H, 4.34; N, 6.03. Found: C, 61.67; H, 4.26; N, 6.05.

***fac*-Ir(*46dfppy*)<sub>3</sub> (Method B):** *fac*-tris(2-(4,6-difluorophenyl)pyridinato,N,C<sup>2'</sup>)iridium(III). Yield: 74%. MS: *m/z* calcd 762.7; found 763. Anal. Calcd for  $C_{33}H_{18}F_6N_3Ir$ : C, 51.97; H, 2.38; N, 5.51. Found: C, 51.92; H, 2.36; N, 5.51.

***fac*-Ir(*ppz*)<sub>3</sub> (Method C):** *fac*-tris(1-phenylpyrazolato,N,C<sup>2'</sup>)iridium(III). Yield: 84%. MS: *m/z* calcd 621.7; found 622. Anal. Calcd for  $C_{27}H_{21}N_6Ir$ : C, 52.16; H, 3.40; N, 13.52. Found: C, 52.04; H, 3.39; N, 13.52.

***fac*-Ir(*dfppz*)<sub>3</sub> (Method B):** *fac*-tris(1-(4,6-difluoro-phenyl)pyrazolato,N,C<sup>2'</sup>)iridium(III). Yield: 78%. MS: *m/z* calcd 729.7; found 730. Anal. Calcd for  $C_{27}H_{15}F_6N_6Ir$ : C, 44.44; H, 2.07; N, 11.52. Found: C, 44.23; H, 1.89; N, 11.28.

***fac*-Ir(*tfmppz*)<sub>3</sub> (Method B):** *fac*-tris(1-(4-trifluoromethylphenyl)pyrazolato,N,C<sup>2'</sup>)iridium(III). Yield: 72%. MS: *m/z* calcd 789.7; found 790. Anal. Calcd for  $C_{27}H_{18}F_9N_6Ir$ : C, 43.64; H, 2.20; N, 10.18. Found: C, 43.68; H, 2.01; N, 9.90.

***mer*-Ir(*ppy*)<sub>3</sub>:** *mer*-tris(2-(phenyl)pyridinato,N,C<sup>2'</sup>)iridium(III). Yield: 75%. MS: *m/z* calcd 654.8; found 655. Anal. Calcd for  $C_{36}H_{30}N_3Ir$ : C, 60.53; H, 3.69; N, 6.42. Found: C, 60.25; H, 3.59; N, 6.46.

***mer*-Ir(*tpy*)<sub>3</sub>:** *mer*-tris(2-(*p*-tolyl)pyridinato,N,C<sup>2'</sup>)iridium(III). Yield: 78%. MS: *m/z* calcd 696.9; found 697. Anal. Calcd for  $C_{36}H_{30}N_3Ir$ : C, 62.05; H, 4.34; N, 6.03. Found: C, 61.59; H, 4.23; N, 6.04.

***mer*-Ir(*46dfppz*)<sub>3</sub>:** *mer*-tris(2-(4,6-difluorophenyl)pyridinato,N,C<sup>2'</sup>)iridium(III). Yield: 74%. MS: *m/z* calcd 762.7; found 763. Anal. Calcd for  $C_{33}H_{18}F_6N_3Ir$ : C, 51.97; H, 2.38; N, 5.51. Found: C, 50.25; H, 2.35; N, 5.31.

***mer*-Ir(*ppz*)<sub>3</sub>:** *mer*-tris(1-phenylpyrazolato,N,C<sup>2'</sup>)iridium(III). Yield: 80%. MS: *m/z* calcd 621.71; found 622. Anal. Calcd for  $C_{27}H_{21}N_6Ir$ : C, 52.16; H, 3.40; N, 13.52. Found: C, 51.74; H, 3.13; N, 13.28.

***mer*-Ir(*dfppz*)<sub>3</sub>:** *mer*-tris(1-(4,6-difluorophenyl)pyrazolato,N,C<sup>2'</sup>)iridium(III). Yield: 86%. MS: *m/z* calcd 729.7; found 730. Anal. Calcd for  $C_{27}H_{15}F_6N_6Ir$ : C, 44.44; H, 2.07; N, 11.5. Found: C, 44.32; H, 1.95; N, 11.27.

***mer*-Ir(*tfmppz*)<sub>3</sub>:** *mer*-tris(1-(4-trifluoromethylphenyl)pyrazolato,N,C<sup>2'</sup>)iridium(III). Yield: 69%. MS: *m/z* calcd 789.7; found 790. Anal. Calcd for  $C_{27}H_{18}F_9N_6Ir$ : C, 43.64; H, 2.20; N, 10.18. Found: C, 44.0; H, 2.12; N, 9.95.

**Isomerization of *mer*-Ir(*C^N*)<sub>3</sub> to *fac*-Ir(*C^N*)<sub>3</sub>. Thermal Isomerization.** Samples of *mer*-Ir(*C^N*)<sub>3</sub> (100 mg) were refluxed in 10 mL of glycerol under inert atmosphere for 24 h. After the mixture was cooled to room temperature, 100 mL of deionized  $H_2O$  was added, and the mixture was filtered off and washed with several portions of water and allowed to dry. The crude product was flashed chromatographed using a silica/dichloromethane column.

**Photochemical Isomerization.** Samples of *mer*-Ir(*C^N*)<sub>3</sub> (10–15 mg) were dissolved in 0.5 mL of *d*<sub>6</sub>-DMSO in Young's NMR tube (Wilmad Co.). The samples were degassed, and the <sup>1</sup>H NMR spectrum was taken before and after exposure to UV light. Handheld TLC lamps (UVP model UVGL-25) positioned face-to-face and covered with aluminum foil were the UV source. After 2 h, >95% conversion was observed as verified by <sup>1</sup>H NMR spectroscopy.

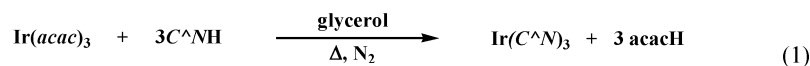
## Results and Discussion

**Synthesis and Structure of Ir(*C^N*)<sub>3</sub> Complexes.** Tris-cyclometalated Ir(III) complexes can be prepared by three different synthetic routes (eqs 1–3, Scheme 1) using either 2-phenylpyridine (*ppy*H) or 1-phenylpyrazole (*ppz*H) as the cyclometalating ligand precursors (Figure 1). The first method involves treating Ir(*acac*)<sub>3</sub> with 3 equiv of the free ligand in glycerol, at refluxing temperatures (Method A, eq 2).<sup>5h</sup> The tris-cyclometalated complexes can also be prepared from the appropriate  $\beta$ -diketonate derivative [(*C^N*)<sub>2</sub>Ir(*O^O*), *O^O* = 2,2,6,6-tetramethyl-3,5-heptanedione (*dpm*)] (Method B) or dichloro-bridged dimer [(*C^N*)<sub>2</sub>Ir( $\mu$ -Cl)<sub>2</sub>Ir(*C^N*)<sub>2</sub>] (Method C), by heating the Ir complex with a 2–3-fold excess of cyclometalating ligand in glycerol. These syntheses work equally well for other pyridine-type ligands (e.g., *tpy*H, *46dfppy*H), as well as for phenylpyrazoles (e.g., *46dfppz*H, *tfmppz*H).

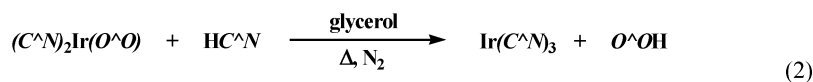
Methods B and C have several advantages over Method A. The dichloro-bridged dimers<sup>28</sup> and (*C^N*)<sub>2</sub>Ir(*O^O*)<sup>8</sup> compounds are easily prepared in high yield from  $IrCl_3 \cdot H_2O$ , a starting material less expensive than Ir(*acac*)<sub>3</sub>. In addition, Methods B

Scheme 1

## METHOD A



## METHOD B



## METHOD C

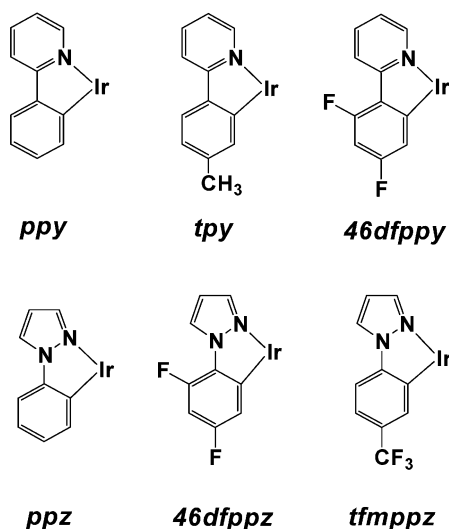
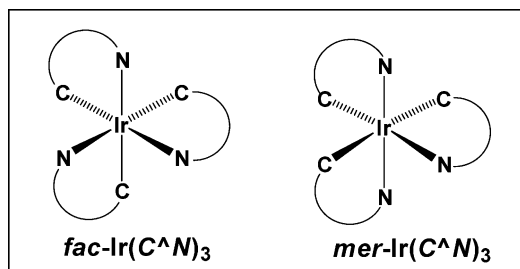
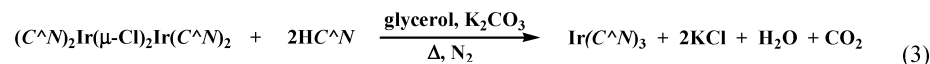


**Figure 1.** Cyclometalating ligands used to prepare  $\text{Ir}(\text{C}^{\wedge}\text{N})_3$ . Abbreviations used throughout the paper are listed below the  $\text{C}^{\wedge}\text{N}$  fragment.

and C give higher yields than does Method A. For example, reactions using Method C and either *ppy*H or *ppz*H give yields between 80 and 85% (based on the starting dimer, reaction temperature  $\sim 200$  °C) versus 45–60% using Method A.<sup>5h,16</sup> Previous routes to make tris-cyclometalated Ir(III) complexes also utilize either  $\text{IrCl}_3 \cdot \text{H}_2\text{O}$  or  $(\text{C}^{\wedge}\text{N})_2\text{Ir}(\mu\text{-Cl})_2\text{Ir}(\text{C}^{\wedge}\text{N})_2$  complexes as starting materials.<sup>6,9a</sup> However, these methods employ a large excess of the cyclometalating precursor ligands as solvent, making it necessary to prepare the desired  $\text{HC}^{\wedge}\text{N}$  compounds on a relatively large scale.

The reaction temperature and nature of the cyclometalating ligand strongly affect the facial/meridional product ratios of the reactions. For the nonfluorinated ligands *ppy*H, *tpy*H, and *ppz*H, both Methods B and C give the facial isomer as the predominant product when reaction temperatures are  $>200$  °C. A small amount of the meridional isomer (typically 1–3%) is sometimes also present in the crude reaction mixture. The meridional

impurity can be readily removed by recrystallization or column chromatography. Higher yields of the *mer*- $\text{Ir}(\text{C}^{\wedge}\text{N})_3$  complexes (68–80%) are obtained using Method C at a lower temperature, that is, 140 °C. Interestingly, different results are obtained with the fluorine-substituted ligands, *46dfppz*H, *tfmppz*H, and *46dfppy*H. All of these ligands give the facial isomer as the major product when Methods A or B are used at high temperature ( $>200$  °C). However, when using Method C, we found that *46dfppz*H and *tfmppz*H give meridional isomers as principal products, whereas *46dfppy*H gives mixtures of *fac*/*mer*-isomers, along with other unidentified products, even at 140 °C. Therefore, pure samples of *mer*- $\text{Ir}(\text{C}^{\wedge}\text{N})_3$  were prepared by Method C using 2-ethoxyethanol as solvent at 120 °C.

The coordination geometry of the precursor complexes used in Method C [ $(\text{C}^{\wedge}\text{N})_2\text{Ir}(\mu\text{-Cl})_2\text{Ir}(\text{C}^{\wedge}\text{N})_2$ ] has the Ir–N bonds in a mutually trans disposition. This suggests that cyclometalation by the third  $\text{C}^{\wedge}\text{N}$  ligand leads directly to the formation of the meridional isomer, as observed when the syntheses are carried out at a lower temperature.<sup>5b</sup> When the reaction temperature for Method C is raised to  $>200$  °C, however, isomerization of either the starting materials or the formed meridional isomers needs to occur to form the observed facial products (*vide infra*).

**NMR Characterization.** The solution structures of the complexes were established using  $^1\text{H}$ ,  $^{13}\text{C}$ , and, where applicable,  $^{19}\text{F}$  NMR spectroscopy. The  $^1\text{H}$  and  $^{19}\text{F}$  NMR spectra of *fac*- and *mer*- $\text{Ir}(\text{C}^{\wedge}\text{N})_3$  are presented in Figure 2; the  $^1\text{H}$  NMR spectra of all of the other complexes are given in the Supporting Information. The facial and meridional isomers of  $\text{Ir}(\text{C}^{\wedge}\text{N})_3$  complexes are readily distinguished by NMR spectroscopy, as all of the derivatives display similar spectral characteristics. In the facial tris-cyclometalates, the three ligands surrounding the iridium atom are magnetically equivalent due to the inherent  $C_3$  symmetry of the complexes. This gives rise to first-order NMR spectra and makes spectral interpretation for these isomers relatively straightforward because the total number of resonances in the complex are equal to the number of resonances in a single anionic  $\text{C}^{\wedge}\text{N}$  ligand. In the  $^1\text{H}$  NMR spectrum of *fac*- $\text{Ir}(\text{C}^{\wedge}\text{N})_3$ , for example, five distinct aromatic proton resonances are displayed, each peak integrating to three equivalent H's that correspond to an individual aromatic proton in the *46dfppz* ligand (Figure 2). In contrast, the  $C_1$  symmetry of the *mer*- $\text{Ir}(\text{C}^{\wedge}\text{N})_3$  complexes gives rise to non-first-order  $^1\text{H}$  NMR spectra with the total of number of resonances equal to the total number of aromatic protons in the complex. Hence, the  $^1\text{H}$  NMR spectrum of the *mer*- $\text{Ir}(\text{C}^{\wedge}\text{N})_3$  is more com-

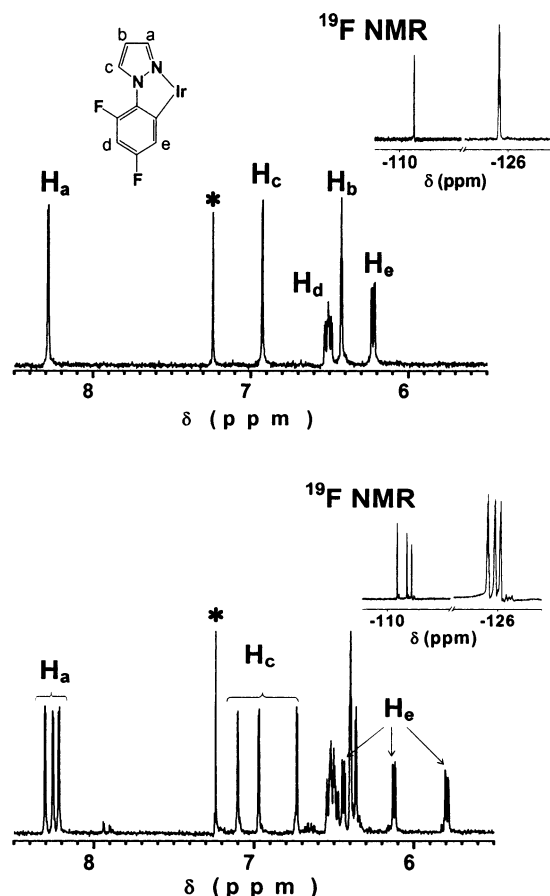


**Figure 2.**  $^1\text{H}$  and  $^{19}\text{F}$  NMR spectra of *fac*-Ir(*46dfppz*)<sub>3</sub> (top) and *mer*-Ir(*46dfppz*)<sub>3</sub> (bottom). The solvent peak is indicated by \*. The  $^{19}\text{F}$  spectra ( $\text{C}_6\text{F}_6$  was used as an external reference  $\delta$  (ppm):  $-164$  ppm) are shown as insets to the  $^1\text{H}$  spectra. The  $^{19}\text{F}$  spectrum of the meridional isomer is shown with a split scale for clarity.

plicated than the facial isomer with 15 distinct aromatic proton resonances appearing in the spectrum, each integrating as a single proton. For example, three aromatic resonances in the facial isomer, labeled  $\text{H}_a$ ,  $\text{H}_c$ , and  $\text{H}_e$  ( $\delta = 8.30, 6.9, 6.2$  ppm, respectively), appear as nine separate resonances in the meridional isomer. Similarly, the  $^1\text{H}$ -decoupled  $^{13}\text{C}$  NMR spectrum of *fac*-Ir(*46dfppz*)<sub>3</sub> displays only nine inequivalent aromatic carbon resonances, whereas 27 carbon resonances are observed for the meridional isomer. The  $^{19}\text{F}$  NMR spectroscopy also clearly distinguishes between the isomers of Ir(*dfppz*)<sub>3</sub> (see insets to Figure 2). The facial isomer shows two distinct fluorine resonances, while the meridional isomer displays six distinct fluorine resonances.

**X-ray Crystallography.** Single crystals of *mer*-Ir(*tpy*)<sub>3</sub>, as well as the facial and meridional isomers of Ir(*ppz*)<sub>3</sub> and Ir(*tfmppz*)<sub>3</sub>, were grown from methanol/dichloromethane solution and characterized using X-ray crystallography. The crystal data are given in Table 1. Tables of atomic coordinates, bond lengths, and angles for each complex are given in the Supporting Information. All of the complexes examined here (both *fac*- and *mer*-isomers) have the three cyclometalating ligands in a pseudooctahedral coordination geometry around the metal center. The C–C and C–N intraligand bond lengths and angles are within normal ranges expected for cyclometalated Ir(III) complexes and are similar to values reported for the ( $\text{C}^{\wedge}\text{N}$ )<sub>2</sub>Ir-( $\mu\text{-Cl}$ )<sub>2</sub>Ir( $\text{C}^{\wedge}\text{N}$ )<sub>2</sub><sup>29</sup> and *fac*-Ir( $\text{C}^{\wedge}\text{N}$ )<sub>3</sub><sup>9a,29</sup> complexes, as well as

**Table 2.** Comparison of Selected Bond Distances ( $\text{\AA}$ ) for *fac*-Ir(*tpy*)<sub>3</sub>, (*tpy*)<sub>2</sub>Ir(*acac*),<sup>8a</sup> and *mer*-Ir(*tpy*)<sub>3</sub>

| bond type | bond distances ( $\text{\AA}$ )           |   |   |
|-----------|---|---|---|
|           | <i>fac</i> -Ir( <i>tpy</i> ) <sub>3</sub> | <i>mer</i> -Ir( <i>tpy</i> ) <sub>3</sub> | ( <i>tpy</i> ) <sub>2</sub> Ir( <i>acac</i> ) |
| Ir–N1     | 2.132(5)                                  | 2.151(9)                                  | 2.023(5)                                      |
| Ir–N2     |   | 2.044(8)                                  |   |
| Ir–N3     |   | 2.065(8)                                  |   |
| Ir–C1     | 2.024(6)                                  | 2.076(10)                                 | 1.985(7)                                      |
| Ir–C2     |   | 2.086(12)                                 |   |
| Ir–C3     |   | 2.020(8)                                  |   |

to reported values for other mononuclear complexes with the ( $\text{C}^{\wedge}\text{N}$ )<sub>2</sub>Ir fragment.<sup>30,31</sup>

Figure 3 gives molecular plots for *fac*-Ir(*tpy*)<sub>3</sub>, *mer*-Ir(*tpy*)<sub>3</sub>, and (*tpy*)<sub>2</sub>Ir(*acac*). The Ir–C and Ir–N bond lengths for each of the complexes are given in Table 2. The structural data for *fac*-Ir(*tpy*)<sub>3</sub><sup>29</sup> and (*tpy*)<sub>2</sub>Ir(*acac*)<sup>8a</sup> were taken from literature references. The facial isomer sits on a three-fold axis, leading to identical Ir–C and Ir–N bond lengths of 2.024(6) and 2.132(5)  $\text{\AA}$ , respectively. The bond lengths in the meridional isomer of *tpy* differ markedly from those of the facial isomer. The Ir–C bond trans to a pyridyl group (Ir–C3 = 2.020(8)  $\text{\AA}$ ) shares an electronic environment and, thus, bond length similar to those of the Ir–C bonds of the facial isomer. Likewise, the Ir–N bond trans to the phenyl group (Ir–N1 = 2.151(9)  $\text{\AA}$ ) is nearly the same length as the Ir–N bonds of the facial isomer. The Ir–N bonds of the mutually trans pyridyl groups in the meridional complex (Ir–N2 = 2.044(8)  $\text{\AA}$  and Ir–N3 = 2.065(8)  $\text{\AA}$ ) are significantly shorter than Ir–N bonds of the facial isomer. This is consistent with the weaker trans influence of a pyridyl group relative to a phenyl ligand.<sup>32</sup> In contrast, the Ir–C bonds trans to phenyl groups (Ir–C1 = 2.076(10)  $\text{\AA}$  and Ir–C2 = 2.086(12)  $\text{\AA}$ ) have lengths markedly longer than the Ir–C bonds of the facial isomer, consistent with the significant trans influence of phenyl groups on each other. It is also interesting to compare *mer*-Ir(*tpy*)<sub>3</sub> and (*tpy*)<sub>2</sub>Ir(*acac*) structures. The bis-cyclometalated fragment of (*tpy*)<sub>2</sub>Ir(*acac*) has the same disposition of *tpy* ligands as found in *mer*-Ir(*tpy*)<sub>3</sub>, and the mutually trans disposed Ir–N bonds in both complexes lengths have similar lengths. On the other hand, the weak trans influence of the acetylacetonate ligand leads to shorter Ir–C bonds (av = 1.984(6)  $\text{\AA}$ ) for the (*tpy*)<sub>2</sub>Ir(*acac*) complex than those observed in either the meridional or the facial Ir(*tpy*)<sub>3</sub> complexes.

The structures of the facial and meridional isomers of Ir-(*ppz*)<sub>3</sub> are shown in Figure 4. The Ir–C and Ir–N bond lengths for the two complexes are given in Table 3. The average Ir–C (2.021(6)  $\text{\AA}$ ) and Ir–N (2.124(5)  $\text{\AA}$ ) bond lengths of *fac*-Ir-(*ppz*)<sub>3</sub> are very similar to those of *fac*-Ir(*tpy*)<sub>3</sub>, suggesting a similar trans influence for pyridyl and pyrazolyl groups. In the meridional isomer, the mutually trans Ir–C bond lengths (Ir–C1 and Ir–C2, av = 2.054(2)  $\text{\AA}$ ) are similar to those of *mer*-Ir(*tpy*)<sub>3</sub> and reflect an equivalent degree of trans influence for both aryl groups in the two chelate systems. The mutually trans Ir–N bond lengths (Ir–N1 and Ir–N2, av = 2.019(2)  $\text{\AA}$ ) are

(29) Garces, F. O.; Dedian, K.; Keder, N. L.; Watts, R. J. *Acta Crystallogr.* **1993**, C49, 1117.

(30) Urban, R.; Kramer, R.; Mihan, S.; Polborn, K.; Wagner, B.; Beck, W. *J. Organomet. Chem.* **1996**, 517, 191.

(31) Neve, F.; Crispini, A. *Eur. J. Inorg. Chem.* **2000**, 1039.

(32) Douglas, B.; McDaniel, D.; Alexander, J. *Concepts and Models in Inorganic Chemistry*, 3rd ed.; John Wiley & Sons, Inc.: New York, 1994.



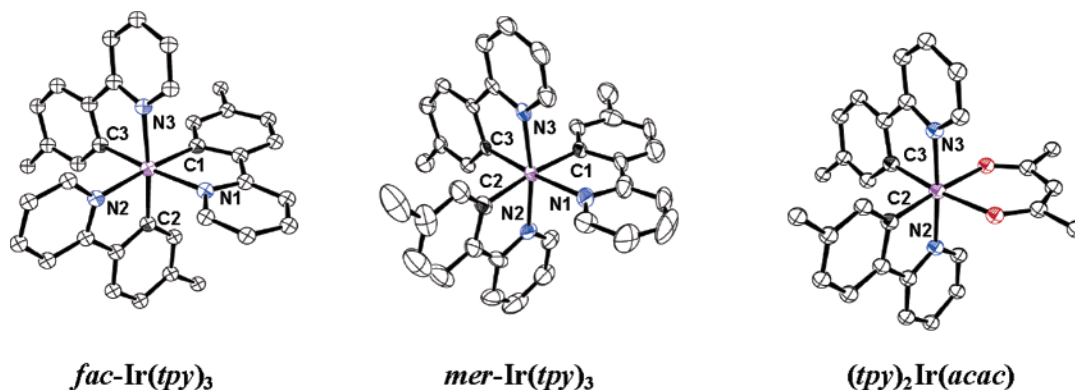


**Figure 3.** ORTEP drawings of *fac*-Ir(*tpy*)<sub>3</sub>, *mer*-Ir(*tpy*)<sub>3</sub>, and (*tpy*)<sub>2</sub>Ir(*acac*). The thermal ellipsoids for the image represent 25% probability limit. The hydrogen atoms have been omitted for clarity.

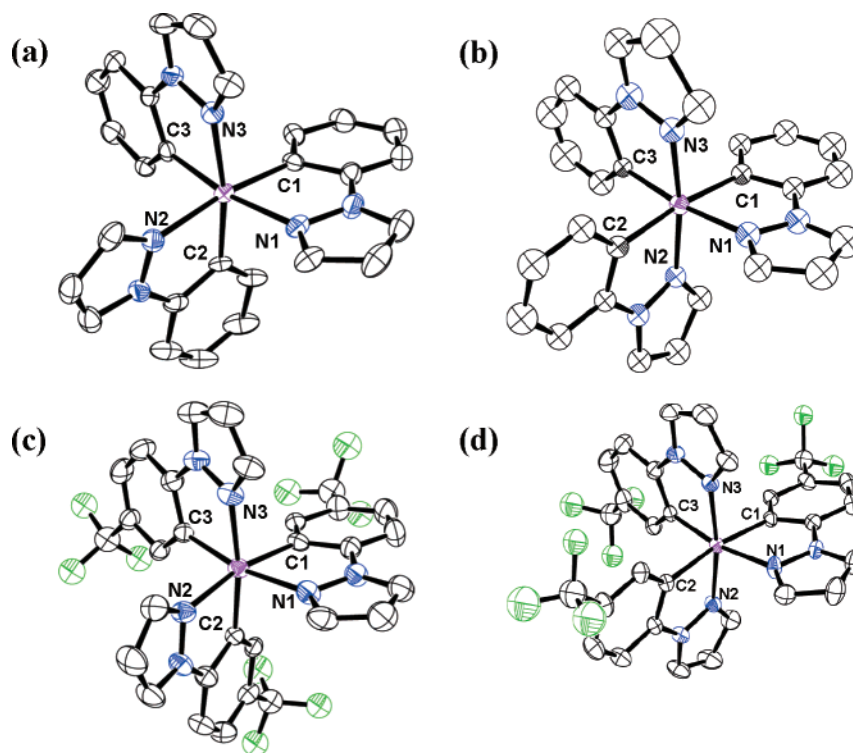


**Figure 4.** ORTEP drawings of (a) *fac*-Ir(*ppz*)<sub>3</sub>, (b) *mer*-Ir(*ppz*)<sub>3</sub>, (c) *fac*-Ir(*tfmppz*)<sub>3</sub>, and (d) *mer*-Ir(*tfmppz*)<sub>3</sub>.

**Table 3.** Selected Bond Distances (Å) and Angles (deg) for *fac*-Ir(*ppz*)<sub>3</sub>, *mer*-Ir(*ppz*)<sub>3</sub>, *fac*-Ir(*tfmppz*)<sub>3</sub>, and *mer*-Ir(*tfmppz*)<sub>3</sub>

| bond type          | Ir( <i>ppz</i> ) <sub>3</sub> |            | Ir( <i>tfmppz</i> ) <sub>3</sub> |            |
|--------------------|-------------------------------|------------|----------------------------------|------------|
|                    | facial                        | meridional | facial                           | meridional |
| Bond Distances (Å) |                               |            |                                  |            |
| Ir–N1              | 2.117(5)                      | 2.053(2)   | 2.114(7)                         | 2.095(4)   |
| Ir–N2              | 2.135(5)                      | 2.026(2)   | 2.113(7)                         | 2.024(5)   |
| Ir–N3              | 2.120(6)                      | 2.013(2)   | 2.116(8)                         | 2.016(5)   |
| Ir–C1              | 2.015(7)                      | 2.051(2)   | 2.016(8)                         | 2.073(5)   |
| Ir–C2              | 2.027(6)                      | 2.057(2)   | 2.016(8)                         | 2.083(5)   |
| Ir–C3              | 2.021(6)                      | 1.993(2)   | 2.013(8)                         | 1.991(5)   |
| Bond Angles (deg)  |                               |            |                                  |            |
| N2–Ir–N3           | 94.4(2)                       | 171.54(8)  | 95.1(3)                          | 171.26(17) |
| C1–Ir–C2           | 93.7(3)                       | 172.67(9)  | 93.7(3)                          | 170.9(2)   |

also similar to values for the corresponding bonds in *mer*-Ir(*tpy*)<sub>3</sub> consistent with pyrazole having a trans influence comparable to that of pyridine. However, the bond lengths for Ir–C trans to pyrazolyl (1.993(2) Å) and Ir–N trans to phenyl (2.053 Å) are shorter than the corresponding pair in *mer*-Ir(*tpy*)<sub>3</sub>, as

well as to the Ir–C and Ir–N bonds in the facial isomer. This decrease in bond distance is most likely due to less steric repulsion between the *ppz* ligands when the complex is in a meridional configuration.

The structures of the facial and meridional isomers of Ir(*tfmppz*)<sub>3</sub> are shown in Figure 4, and the Ir–C and Ir–N bond lengths are given in Table 3. The electron-accepting trifluoromethyl group of the *tfmppz* ligand is in a meta disposition relative to Ir and, electronically, is thus weakly coupled to the metal center. Hence, the average Ir–C (2.015(8) Å) and Ir–N (2.114(7) Å) bond lengths for the facial Ir(*tfmppz*)<sub>3</sub> are the same as those observed for the facial isomers of both Ir(*tpy*)<sub>3</sub> and Ir(*ppz*)<sub>3</sub>. For the meridional isomer of Ir(*tfmppz*)<sub>3</sub>, the mutually trans Ir–C bonds (av = 2.078(5) Å) and Ir–N bonds (av = 2.020(5) Å) are similar in length to the equivalent bonds in *mer*-Ir(*tpy*)<sub>3</sub> and *mer*-Ir(*ppz*)<sub>3</sub>. The Ir–C trans to pyrazolyl (1.991(5) Å) and Ir–N trans to phenyl (2.095(4) Å) bond lengths are also similar to values for the corresponding bonds in the meridional *tpy* and *ppz* complexes. Likewise, the bond distances



**Table 4.** Photophysical and Electrochemical Properties of Ir(C<sup>^</sup>N)<sub>3</sub> Complexes

| complex        | absorption <sup>a</sup><br>λ (nm) {ε, 10 <sup>3</sup> L mol <sup>-1</sup> cm <sup>-1</sup> } | emission at 77 K <sup>b</sup> |        | emission at 298 K |        | redox (V) <sup>c</sup>         |                                 |
|----------------|--|-------------------------------|--------|-------------------|--------|--------------------------------|---------------------------------|
|                |  | λ <sub>max</sub>              | τ (μs) | λ <sub>max</sub>  | τ (μs) | E <sub>1/2</sub> <sup>ox</sup> | E <sub>1/2</sub> <sup>red</sup> |
| <i>ppy</i>     |  |                               |        |                   |        |                                |                                 |
| <i>fac</i>     | 244 (45.5), 283 (44.8), 341 (9.2), 377 (12.0), 405 (8.1), 455 (2.8), 488 (1.6)               | 492                           | 3.6    | 510               | 1.9    | 0.31                           | -2.70, -3.00                    |
| <i>mer</i>     | 246 (47.3), 276 (51.0), 339 (9.2), 382 (10.7), 410 (7.2), 457 (3.4), 488 (1.4)               | 493                           | 4.2    | 512               | 0.15   | 0.25                           | -2.63, -2.82                    |
| <i>tpy</i>     |  |                               |        |                   |        |                                |                                 |
| <i>fac</i>     | 248 (41.4), 287 (44.7), 347 (10.6), 374 (11.8), 410 (7.0), 450 (2.9), 485 (1.4)              | 492                           | 3.0    | 510               | 2.0    | 0.30                           | -2.78, -3.09                    |
| <i>mer</i>     | 276 (53.6), 336 (13.4), 383 (8.4), 420 (5.3), 451 (3.7), 485 (1.5)                           | 530 <sup>d</sup>              | 4.8    | 550               | 0.26   | 0.18                           | -2.73, -3.04                    |
| <i>46dfppy</i> |  |                               |        |                   |        |                                |                                 |
| <i>fac</i>     | 240 (50.2), 274 (44.7), 292 (25.5), 346 (11.3), 379 (7.1), 427 (1.6), 457 (0.3)              | 450                           | 2.5    | 468               | 1.6    | 0.78                           | -2.51, -2.81                    |
| <i>mer</i>     | 264 (50.7), 312 (15.5), 353 (8.8), 388 (7.8), 428 (2.5), 456 (0.9)                           | 460                           | 5.4    | 482               | 0.21   | 0.69                           | -2.50, -2.86                    |
| <i>ppz</i>     |  |                               |        |                   |        |                                |                                 |
| <i>fac</i>     | 244 (49.1), 261 (41.1), 292 (16.5), 321 (13.5), 366 (4.2)                                    | 414                           | 14     |                   |        | 0.39                           |                                 |
| <i>mer</i>     | 228 (44.8), 246 (44.0), 293 (17.3), 320 (9.6), 349 (5.1)                                     | 427 <sup>d</sup>              | 28     |                   |        | 0.28                           |                                 |
| <i>46dfppz</i> |  |                               |        |                   |        |                                |                                 |
| <i>fac</i>     | 246 (55.3), 254 (49.9), 283 (23.1), 316 (10.0)   | 390 <sup>d</sup>              | 27     |                   |        | 0.80                           |                                 |
| <i>mer</i>     | 244 (48.0), 278 (24.0), 322 (8.9)  | 402 <sup>d</sup>              | 33     |                   |        | 0.72                           |                                 |
| <i>tjmpz</i>   |  |                               |        |                   |        |                                |                                 |
| <i>fac</i>     | 243 (45.3), 251 (40.8), 261 (37.0), 289 (12.2), 323 (10.6), 364 (3.6)                        | 422                           | 17     | 428               | 0.05   | 0.73                           |                                 |
| <i>mer</i>     | 234 (42.3), 247 (46.6), 287 (19.4), 344 (7.7), 372 (3.2)                                     | 430 <sup>d</sup>              | 32     |                   |        | 0.62                           |                                 |

<sup>a</sup> Absorption measurements of complexes were taken in CH<sub>2</sub>Cl<sub>2</sub>. <sup>b</sup> 77 K emission and lifetime measurements were carried out in 2-methyltetrahydrofuran. <sup>c</sup> Redox measurements were carried out in anhydrous DMF solution; values are reported relative to Cp<sub>2</sub>Fe/Cp<sub>2</sub>Fe<sup>+</sup>. <sup>d</sup> The λ<sub>max</sub> values correspond to the highest energy peak in the spectrum. See Supporting Information.

for the trans disposed phenyl and pyrazolyl groups are relatively unperturbed by the CF<sub>3</sub> substituent.

**DFT Calculations.** B3LYP density functional theory (DFT) calculations were carried out on all of the Ir(C<sup>^</sup>N)<sub>3</sub> complexes using the Titan software package (Wavefunction, Inc.) with a LACVP\*\* basis set. A similar approach has been used to investigate the ground- and excited-state properties of cyclometalated Ir and Pt compounds.<sup>33,34</sup> The HOMO and LUMO surfaces for *fac*- and *mer*-Ir(*ppz*)<sub>3</sub> are illustrated in the Supporting Information. The discussion here will focus on the results for *fac*- and *mer*-Ir(*ppz*)<sub>3</sub>; however, all of the examined facial and meridional isomers give a similar picture for the HOMO and LUMO orbitals. The calculated values for the Ir–C (2.17 Å) and Ir–N (2.04 Å) bond distances and N–Ir–N (96.3°) and C–Ir–C (95.2°) bond angles are comparable to the experimental values determined in the X-ray structure of *fac*-Ir(*ppz*)<sub>3</sub> (see Table 3). Likewise, the calculated Ir–C and Ir–N bond lengths of *mer*-Ir(*ppz*)<sub>3</sub> have the same length alternations as those observed in the X-ray structure. The calculated HOMO energies for *fac*- and *mer*-Ir(*ppz*)<sub>3</sub> are -5.02 and -4.81 eV, respectively. The HOMO pictures for both isomers consist of a mixture of phenyl and Ir orbitals. The HOMO in the *fac*-isomer is distributed equally among the three *ppz* ligands due to the C<sub>3</sub> symmetry of the complex. The HOMO of the *mer*-isomer is localized primarily on the two *ppz* ligands with the transoid disposition of nitrogen. Similarly, the LUMO – while predominantly phenylpyrazolyl in character – is delocalized among the three ligands in the *fac*-isomer (-0.57 eV) as opposed to being localized on a single ligand in the *mer*-isomer (-0.60 eV). The triplet HSOMOs (HSOMO = highest singly occupied molecular orbital) are calculated to be -1.60 and -1.53 eV for the *fac*- and *mer*-isomer, respectively. The triplet state energy can then be estimated as the difference between the ground-state singlet (HOMO) and triplet (HSOMO) energies.<sup>33,34</sup> The values obtained for the theoretical triplet energy are 3.42 eV (362 nm) for *fac*-Ir(*ppz*)<sub>3</sub> and 3.28 eV (378 nm) for the meridional isomer.

These values are in close agreement with the data obtained from photophysical measurements (vide infra). The calculation results for other tris-cyclometalated Ir complexes will be discussed in the following text as they pertain to electrochemical and spectral interpretation.

**Electrochemistry.** The electrochemical properties of the tris-cyclometalated iridium complexes were examined by cyclic voltammetry. A summary of the redox potentials, measured relative to an internal ferrocene reference (Cp<sub>2</sub>Fe/Cp<sub>2</sub>Fe<sup>+</sup> = 0.45V vs SCE in DMF solvent),<sup>23</sup> is given in Table 4. All of the complexes show reversible oxidation, with potentials of 0.30–0.80 V. The phenylpyridyl-based derivatives exhibit reversible reduction, in the range from -2.51 to -2.78V. However, no reduction is observed for the phenylpyrazolyl-based complexes out to -3.0 V (the solvent limit in DMF). The DFT calculations suggest that the reductive process is largely localized on the heterocyclic portion of the cyclometalating ligands. The reductive electrochemistry of the Ir(C<sup>^</sup>N)<sub>3</sub> complexes is thus consistent with the pyrazolyl being significantly more difficult to reduce than a pyridyl group. The absence of reductive processes in pyrazolyl ligated complexes is a common occurrence noted by other research groups.<sup>35–38</sup> For example, neither Pt(II) nor Rh(III) phenylpyrazolyl cyclometalates undergo measurable reduction, unlike the phenylpyridyl analogues.<sup>6,34</sup>

Replacing the pyridyl moiety with a pyrazolyl group also affects the oxidation potentials of the metal complexes. The oxidation potential of *fac*-Ir(*ppz*)<sub>3</sub> (0.39 V) is shifted to a slightly higher potential than that of *fac*-Ir(*ppy*)<sub>3</sub> (0.31 V). The DFT calculations show that the HOMOs of all of the tris-cyclometalated complexes examined here are composed of Ir-d and phenyl-π orbitals, similar to related studies.<sup>33</sup> While the pyridyl and pyrazolyl ligands do not contribute markedly to the HOMO,

(33) Hay, P. J. *J. Phys. Chem. A* **2002**, *106*, 1634.

(34) Brooks, J.; Babayan, Y.; Lamansky, S.; Djurovich, P. I.; Tsyba, I.; Bau, R.; Thompson, M. E. *Inorg. Chem.* **2002**, *41*, 3055.

(35) Sandrini, D.; Maestri, M.; Ciano, M.; Balzani, V.; Lueoend, R.; Deuschel-Cornioley, C.; Chassot, L.; Von Zelewsky, A. *Gazz. Chim. Acta* **1988**, *118*, 661.

(36) Maeder, U.; Stoeckli-Evans, H.; von Zelewsky, A. *Helv. Chim. Acta* **1992**, *73*, 1321.

(37) Sandrini, D.; Maestri, M.; Ciano, M.; Maeder, U.; von Zelewsky, A. *Helv. Chim. Acta* **1990**, *73*, 1307.

(38) Chassot, L.; von Zelewsky, A. *Inorg. Chem.* **1987**, *26*, 2814.

they do affect the energies of the metal orbitals through  $\pi$ -back-bonding. Previous studies with neutral pyrazole ligands and deprotonated pyrazoles have indicated that the pyrazolyl ligands are weak  $\pi$ -acceptors similar to pyridyl ligands.<sup>19,39</sup> A similar observation has been reported for analogous Pt complexes; Pt(*phpz*)<sub>2</sub> has a higher oxidation potential than Pt(*ppy*)<sub>2</sub> (0.49 and 0.26 V, respectively).<sup>38</sup> In accord with other studies, fluoro and/or trifluoromethyl substituents also increase the oxidation potential of the complexes while simultaneously making the phenylpyridyl-based derivatives easier to reduce.<sup>5h,9,34</sup>

The meridional tris-cyclometalates have oxidation potentials ca. 50–100 mV less positive than their facial isomers, while the reduction potentials for the *mer*-phenylpyridyl-based complexes are only slightly less negative than those in the *fac*-analogues. As mentioned above, the oxidation processes involve the Ir-phenyl center, while reduction occurs primarily on the heterocyclic portion of the C<sup>N</sup> ligands.<sup>40</sup> The difference in electrochemical behavior between the meridional and facial isomers can be explained by the presence of mutually trans phenyl ligands in the *mer*-isomers. This configuration leads to a lengthening of the transoid Ir–C bonds and, consequently, destabilizes the HOMO to a significant extent, while only slightly stabilizing the LUMO. The electrochemistry is in accordance with results from DFT calculations that suggest that the HOMO energies of the meridional isomers are higher than those of the facial forms, while the LUMO energies are roughly the same. For example, the calculated HOMO energy for *mer*-Ir(*tpy*)<sub>3</sub> is –4.67 versus –4.78 eV for *fac*-Ir(*tpy*)<sub>3</sub>, while the LUMO energies are less strongly perturbed (–1.18 versus –1.12 eV, respectively). Therefore, on the basis of these calculations, we predicted that it should be easier to both oxidize and reduce *mer*-Ir(*tpy*)<sub>3</sub> than would be the case for *fac*-Ir(*tpy*)<sub>3</sub>, as is indeed observed.

**Electronic Spectroscopy.** The absorption and emission spectra were recorded for all of the complexes. These data are summarized in Table 4, and spectra for *fac/mer*-Ir(*tpy*)<sub>3</sub> and *fac/mer*-Ir(*ppz*)<sub>3</sub> are given in Figure 5. The photophysical properties of the facial isomers of the phenylpyridyl-based Ir(III) cyclometalates have been examined by a number of research groups.<sup>5,6,9</sup> The absorption spectra of these compounds show intense bands appearing in the ultraviolet part of the spectrum between 240 and 350 nm. These bands have been assigned to the spin-allowed  $^1(\pi \rightarrow \pi^*)$  transitions of the phenylpyridyl ligand. The  $^1(\pi \rightarrow \pi^*)$  bands are accompanied by weaker, lower energy features extending into the visible region from 350 to 450 nm that have been assigned to both allowed and spin-forbidden MLCT transitions. The high intensity of these MLCT bands has been attributed to an effective mixing of these charge-transfer transitions with higher lying spin-allowed transitions on the cyclometalating ligand.<sup>6</sup> This mixing is facilitated by the strong spin–orbit coupling of the Ir(III) center. The absorption spectra for all of the phenylpyrazolyl-based Ir complexes investigated here also show intense bands appearing in the ultraviolet part of the spectrum between 240 and 350 nm. The measured energies and extinction coefficients are comparable to those of the free ligands, that is, *ppz*H, *46dfppz*H, and *fmppz*H. Thus, these features are similarly assigned to the

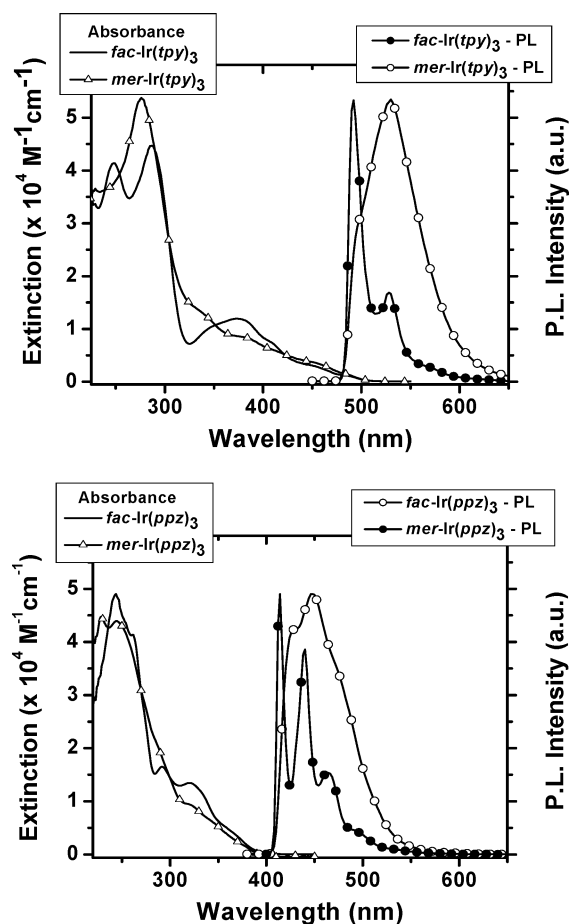


**Figure 5.** Absorption and emission spectra for facial and meridional isomers of Ir(*tpy*)<sub>3</sub> (top) and Ir(*ppz*)<sub>3</sub> (bottom). The absorption spectra were measured in CH<sub>2</sub>Cl<sub>2</sub> at room temperature, and the emission spectra were measured at 77 K in 2-methyltetrahydrofuran (2-MeTHF) glass.

allowed  $^1(\pi \rightarrow \pi^*)$  transitions of the phenylpyrazolyl-based ligands.<sup>41</sup> These bands, as in the phenylpyridyl-based analogues, are also accompanied by weaker, low-lying charge-transfer transitions at 350–380 nm. However, the MLCT transitions of the phenylpyrazolyl-based complexes are significantly higher in energy than those of phenylpyridyl analogues. A similar hypsochromic shift has also been observed in the absorption spectra of phenylpyrazolyl-based Rh<sup>36,37</sup> and Pt<sup>35,38</sup> cyclometalates, as well as in pyridylpyrazolyl-based Ru tris-chelates.<sup>18,19</sup> The shift to higher energy indicates an increase in energy separation between the metal d- and  $\pi^*$ -orbitals and is principally due to the fact that the  $\pi^*$ -orbitals of pyrazole are higher in energy than the  $\pi^*$ -orbitals of pyridine.<sup>18,19,39</sup>

The facial isomers of the phenylpyridyl-based complexes are all intensely luminescent, both at 77 K and at room temperature (Table 4), with emission characteristic of phosphorescence from a mixed-ligand-centered-MLCT (LC-MLCT) triplet state.<sup>6,8,34</sup> The photophysical properties of *fac*-Ir(*tpy*)<sub>3</sub> at 77 K ( $\lambda_{\max} = 492$  nm,  $\tau = 3.0$   $\mu$ s) are nearly the same as those of *fac*-Ir(*ppy*)<sub>3</sub>, while the difluoro-substituted analogue, *fac*-Ir(*46dfppy*)<sub>3</sub>, has a blue-shifted emission ( $\lambda_{\max} = 450$  nm,  $\tau = 2.5$   $\mu$ s). The

(39) Sullivan, P.; Salmon, D. J.; Meyer, T. J.; Peeding, J. *Inorg. Chem.* **1979**, *18*, 3369.

(40) Kulikova, M.; Balashev, K. P.; Kvam, P. I.; Songstad, J. *Russ. J. Gen. Chem.* **2000**, *70*, 163.

(41) (a) Pavlik, J. W.; Connors, R. E.; Burns, D. S.; Kurzweil, E. M. *J. Am. Chem. Soc.* **1993**, *115*, 7645. (b) Cativiela, C.; Laureiro, J. I. G.; Elguero, J.; Elguero, E. *Gazz. Chim. Ital.* **1991**, *121*, 477. (c) Cativiela, C.; Laureiro, J. I. G.; Elguero, J.; Elguero, E. *Gazz. Chim. Ital.* **1989**, *119*, 41. (d) Cativiela, C.; Laureiro, J. I. G.; Elguero, J.; Elguero, E. *Gazz. Chim. Ital.* **1986**, *116*, 119.

large hypsochromic shift caused by 4,6-difluoro substitution is consistent with behavior seen in Pt(II) cyclometalates.<sup>34</sup> Substitution of the phenyl hydrogens with inductively electron-withdrawing fluorine atoms, particularly on the 4'- and 6'-positions, stabilizes the HOMO more than the LUMO, thus increasing the triplet energy gap.<sup>34</sup>

In contrast to the phenylpyridyl-based complexes, the facial isomers of the phenylpyrazolyl-based compounds are all very weak emitters at room temperature ( $\Phi < 0.1\%$ ), but are intensely luminescent at 77 K. Several related *ppz* cyclometalated Pt and Rh complexes have also been reported to be poorly emissive in fluid solution but highly emissive in glassy matrixes at 77 K.<sup>35,36</sup> The highly structured emissions of the facial phenylpyrazolyl-based complexes occur at higher energies and have longer lifetimes than the phenylpyridyl-based analogues. For example, at 77 K, the emission for *fac*-Ir(*ppz*)<sub>3</sub> has a  $\lambda_{\text{max}} = 414$  nm and  $\tau = 14$   $\mu\text{s}$ , while for *fac*-Ir(*ppy*)<sub>3</sub>, the values are  $\lambda_{\text{max}} = 492$  nm and  $\tau = 3.6$   $\mu\text{s}$ . The behavior is consistent with a strongly perturbed ligand-centered transition in the phenylpyrazolyl derivatives. The triplet energy of the *C^N* ligand strongly influences the phosphorescence energy of the corresponding cyclometalate because the excited state has both MLCT and intraligand ( $\pi \rightarrow \pi^*$ ) triplet character.<sup>6,8</sup> The triplet energy of phenylpyrazole (378 nm, 26 500  $\text{cm}^{-1}$ )<sup>36,41</sup> is greater than that of phenylpyridine (430 nm, 23 300  $\text{cm}^{-1}$ );<sup>42</sup> therefore, a phenylpyrazolyl-based cyclometalate is expected to have a higher emission energy than a related phenylpyridyl-based complex. Also, as seen with the phenylpyridyl-based complexes,<sup>5,34</sup> addition of electron-withdrawing fluorine substituents on the phenyl ring of *ppz* blue-shifts the emission for the corresponding cyclometalated complexes; thus, the triplet energy of *fac*-Ir(*46dfppz*)<sub>3</sub> is 390 nm. To our knowledge, this is the first Ir(III) tris-cyclometalate that emits in the ultraviolet region (below 400 nm).

The meridional isomers of the tris-cyclometalates exhibit photophysical characteristics different from those of their facial analogues. For example, the  $^1(\pi \rightarrow \pi^*)$  absorption in *mer*-Ir(*tpy*)<sub>3</sub> (Figure 5a) occurs as a single intense band at 276 nm, whereas in *fac*-Ir(*tpy*)<sub>3</sub> it appears as two features at 248 and 287 nm. Likewise, the MLCT band shapes in the meridional isomer are less sharply defined and have lower extinctions than those in the facial isomer. Greater differences exist in the luminescent behavior. Unlike the highly structured emission displayed by *fac*-isomers, the *mer*-isomers display broader, red-shifted luminescence. At room temperature, the *mer*-isomers of the phenylpyridyl derivatives also have much lower luminescent efficiencies and, concomitantly, shorter emission decay lifetimes than their facial counterparts. Assuming that the emitting state of a complex is formed with unit efficiency, one can calculate the radiative ( $k_r$ ) and nonradiative ( $k_{nr}$ ) rate constants using the relationships  $k_r = \Phi_{\text{PL}}/\tau$  and  $\Phi_{\text{PL}} = k_r/(k_r + k_{nr})$ . The calculated radiative and nonradiative rate constants for the phenylpyridyl-based complexes are listed in Table 5. The *fac*- and *mer*-isomers have similar radiative rate constants; however, the nonradiative rate constants for the *mer*-isomers are more than an order of magnitude larger than those of the *fac*-isomers. The nonradiative rate constant is a sum of rates for several processes that quench emission. One of these

**Table 5.** Luminescent Quantum Efficiencies, Lifetimes, and the Radiative/Nonradiative Decay Rates for Ir(*C^N*)<sub>3</sub> Complexes at Room Temperature

| complex                                       | $\Phi_{\text{PL}}$ | $\tau$ ( $\mu\text{s}$ ) | $k_r$             | $k_{nr}$          |
|---|--------------------|--------------------------|-------------------|-------------------|
| <i>fac</i> -Ir( <i>ppy</i> ) <sub>3</sub>     | 0.40               | 1.9                      | $2.1 \times 10^5$ | $3.2 \times 10^5$ |
| <i>mer</i> -Ir( <i>ppy</i> ) <sub>3</sub>     | 0.036              | 0.15                     | $2.4 \times 10^5$ | $6.4 \times 10^6$ |
| <i>fac</i> -Ir( <i>tpy</i> ) <sub>3</sub>     | 0.50               | 2.0                      | $2.5 \times 10^5$ | $2.5 \times 10^5$ |
| <i>mer</i> -Ir( <i>tpy</i> ) <sub>3</sub>     | 0.051              | 0.26                     | $2.0 \times 10^5$ | $3.6 \times 10^6$ |
| <i>fac</i> -Ir( <i>46dfppy</i> ) <sub>3</sub> | 0.43               | 1.6                      | $2.7 \times 10^5$ | $3.6 \times 10^5$ |
| <i>mer</i> -Ir( <i>46dfppy</i> ) <sub>3</sub> | 0.053              | 0.21                     | $2.5 \times 10^5$ | $4.5 \times 10^6$ |

processes could involve bond dissociation in the excited state. The mutually trans Ir–C<sub>1</sub> and Ir–C<sub>2</sub> bonds in the *mer*-Ir(*tpy*)<sub>3</sub> are already significantly longer than those of the facial analogue as a result of the strong trans influence of phenyl groups. The broadened emission of the *mer*-isomers indicates that the excited-state geometry is further distorted from that of the ground state. Photolytic cleavage of either an Ir–C or an Ir–N bond can then lead to subsequent rearrangement of the complex. This sort of bond breaking in the excited state is most likely responsible for the photoisomerization process described below.

***mer*-to-*fac* Isomerization.** The fact that the meridional Ir(*C^N*)<sub>3</sub> isomers can be obtained in good yield at low temperature, via synthetic Method C, suggests that the meridional isomers are kinetically favored products, while the facial isomers, obtained at higher temperatures, are thermodynamically favored. To test this hypothesis, the thermal conversion of meridional to facial isomers was examined. A pure sample of *mer*-Ir(*tpy*)<sub>3</sub> was dissolved in glycerol and refluxed for 24 h. Subsequent purification by column chromatography, under conditions where the facial and meridional isomers are cleanly separated, gave only a single colored band, and pure *fac*-Ir(*tpy*)<sub>3</sub> was isolated in >70% yield. This result supports the hypothesis that the meridional isomer is the kinetically favored product and converts to the facial isomer during high-temperature synthesis. The *mer*-Ir(*ppy*)<sub>3</sub>, *mer*-Ir(*ppz*)<sub>3</sub>, *mer*-Ir(*46dfppz*)<sub>3</sub>, and *mer*-Ir(*tfmppz*)<sub>3</sub> complexes also isomerize to their facial forms using the same reaction conditions. However, the *mer*-Ir(*46dfppy*)<sub>3</sub> complex did not isomerize under these conditions, indicating that a larger kinetic barrier needs be overcome to isomerize this derivative.

The large nonradiative rate constants determined for some of the *mer*-isomers suggest that a bond rupture process may occur in the excited state; hence, the photostability of *mer*-Ir(*C^N*)<sub>3</sub> complexes was also examined. The <sup>1</sup>H NMR spectra of the samples of the meridional complexes in degassed DMSO-*d*<sub>6</sub> were taken before and after irradiation of the sample with a handheld UV lamp. Nearly complete conversion (>95%) to the corresponding facial isomers was found to occur after less than 2 h of irradiation. This photochemical *mer*-to-*fac* conversion was observed for all of the Ir(*C^N*)<sub>3</sub> complexes reported here. The photoisomerization process is slower in less-coordinating solvents; thus, a sample of *mer*-Ir(*tpy*)<sub>3</sub> in toluene-*d*<sub>8</sub> took 72 h to undergo a similar degree of conversion to the *fac*-isomer. No intermediate species were observed when the NMR spectrum of this sample was examined at various time intervals during the photolysis (see Supporting Information). A clean *mer*-to-*fac* isomerization process is also indicated from the observation of isobestic points in the absorption spectra of *mer*-Ir(*tpy*)<sub>3</sub>, taken at various stages of the photolysis in 2-methyltetrahydrofuran (see Supporting Information).

(42) Murov, S. L.; Carmichael, I.; Hug, G. L. *Handbook of Photochemistry*; Marcel Dekker, Inc.: New York, 1993.



The greater thermodynamic stability of the *fac*-Ir( $C^{\wedge}N$ )<sub>3</sub> complexes relative to the *mer*-isomers can be contrasted to the greater stability of *mer*-Ru(*btpz*)<sub>3</sub> [*btpz* = 1-(2'-(4',5'-benzothiazolyl)pyrazolyl)]<sup>19</sup> and *mer*-Al(8-hydroxyquinolyl)<sub>3</sub><sup>43</sup> relative to their respective facial analogues. This has been attributed to the relief of steric interactions in the latter *mer*-compounds. The differing stability between *fac*- and *mer*-isomers of  $N^{\wedge}N$  and  $C^{\wedge}N$  tris-chelates may be brought about by the preference for maintaining the three strong trans influence phenyl groups of the cyclometalates on the same face of the molecule, trans to the heterocyclic groups. The thermodynamic instability of the meridional configuration is supported by the DFT calculations which show a ~30 kJ/mol stabilization of total energy in favor of the *fac*-isomers.

## Conclusion

The preparative methods for tris-cyclometalates reported here demonstrate that controlling the reaction conditions can impart significant control in the product configuration. For all of the cyclometalating ligands studied here, there is a preference to form the facial isomers at high temperatures (>200 °C) and the meridional isomers at lower temperatures (<150 °C). At high temperatures, the meridional isomer can be efficiently converted to the facial form, demonstrating the facial isomer is the thermodynamic product and the meridional form is the kinetic product. The differences in the ligand configuration of these complexes result in significantly different electrochemical and photophysical properties. The meridional isomers are easier to oxidize, and the emission is broad and red-shifted relative to the facial forms. The solution photoluminescent quantum efficiencies of the meridional isomers and their emission lifetimes are significantly lower than the facial isomers of the same cyclometalating ligands. The large difference between the quantum efficiencies of the meridional and facial isomers can be explained by an efficient bond breaking process for the

meridional excited state, acting as an effective quenching pathway and giving subsequent isomerization to the facial form.

The photochemical isomerization of meridional Ir( $C^{\wedge}N$ )<sub>3</sub> complexes provides a new route to prepare the facial isomers, at temperatures much lower than conditions previously employed to make these complexes. This synthetic procedure can then lead to more efficient utilization of the iridium precursor materials because high reaction temperatures can promote undesired side reactions, decreasing product yields. Also, many potentially interesting and useful cyclometalating ligands have substituents that are unstable in the harsh reaction conditions required by the prior synthetic methods. Therefore, a greater variety of compounds can now be considered as potential ligands for facial tris-cyclometalated iridium complexes. In addition to the synthetic utility of these reactions, the mechanisms of the thermal and photochemical *mer*-to-*fac* isomerizations are of interest. Investigations into the mechanisms of these isomerization processes are currently being pursued in our laboratories.

**Acknowledgment.** The authors thank Universal Display Corp. and the Defense Advanced Research Projects Agency for financial support of this work.

**Supporting Information Available:** <sup>1</sup>H NMR spectra, <sup>1</sup>H and <sup>13</sup>C NMR chemical shifts and coupling constants, UV-vis absorption and emission spectra, and table of DFT-calculated orbital energies for all of the facial and meridional Ir( $C^{\wedge}N$ )<sub>3</sub> compounds examined here, as well as HOMO and LUMO plots for *fac*- and *mer*-isomers of Ir(*ppz*)<sub>3</sub> and a series of absorption and <sup>1</sup>H NMR spectra showing the photoconversion of *mer*-Ir-(*tpy*)<sub>3</sub> to *fac*-Ir(*tpy*)<sub>3</sub> (PDF). Also included are tables of crystal data, atomic coordinates, bond distances, bond angles, and anisotropic displacement parameters for *mer*-Ir(*tpy*)<sub>3</sub>, *fac*- and *mer*-isomers of Ir(*ppz*)<sub>3</sub>, and *fac*- and *mer*-isomers of Ir(*tfmppz*)<sub>3</sub>, as well as the corresponding CIF files. This material is available free of charge via the Internet at <http://pubs.acs.org>.

JA034537Z

(43) Utz, M.; Chen, C.; Morton, M.; Papadimitrakopoulos, F. *J. Am. Chem. Soc.* **2003**, *125*, 1371.